PERGAMON

Automatica 35 (1999) 1663–1670

www.elsevier.com/locate/automatica

Brief Paper

Dynamical analysis and control of microcantilevers☆

M. Ashhab[a], M.V. Salapaka[b], M. Dahleh[a,*], I. Mezić[a]

[a]*Mechanical Engineering Department, University of California, Santa Barbara, CA 93106, USA*
[b]*Electrical Engineering Department, Iowa State University, Ames, IA 50011, USA*

Received 4 March 1997; revised 11 December 1997; received in final form 19 June 1998

Abstract

In this paper, we study the dynamical behavior of a microcantilever-sample system that forms the basis for the operation of atomic force microscopes (AFM). We model the microcantilever by a single mode approximation and the interaction between the sample and cantilever by a van der Waals (vdW) potential. The cantilever is vibrated by a sinusoidal input, and its deflection is detected optically. We analyze the forced dynamics using Melnikov method, which reveals the region in the space of physical parameters where chaotic motion is possible. In addition, using a proportional and derivative controller we compute the Melnikov function in terms of the parameters of the controller. Using this relation it is possible to design controllers that will remove the possibility of chaos. © 1999 Elsevier Science Ltd. All rights reserved.

Keywords: Atomic force microscopy; Chaotic behavior; Melnikov method; Microcantilevers

1. Introduction

Surfaces at the atomic level can be probed with good accuracy using the atomic force microscope (AFM) which was invented in 1986. This is done by moving the sample beneath a tip attached to a soft cantilever which causes the cantilever to deflect. The cantilever deflection is measured by optical methods and is used as an indicator of the force variation on the sample. The behavior of the cantilever depends on the interaction force between its tip and the sample, the spring force which is due to the cantilever, and the equilibrium position of the tip in the absence of the interaction forces. Many cantilever-based instruments are now available which can be used for force measurements, magnetic spin detection, and thermal measurements (Sarid, 1994). All of these instruments share this basic mechanism of a microcantilever interacting with a sample.

It has been experimentally observed that the motion of the cantilever can be chaotic under certain physical conditions (Burnham, Kulik, Gremaud & Briggs, 1995). This type of irregular motion is highly undesirable for the AFM performance since it causes the AFM to give inaccurate measurements. This paper is concerned with the modeling, analysis and control of a typical cantilever–sample interaction, which as was mentioned above is at the heart of the detection scheme employed by AFMs. The objective is to ensure good performance of the microscope by identifying and subsequently eliminating the possibility of chaotic motion of the cantilever. In this work, we show that based on a certain model approximation of the cantilever–sample system it is possible to design controllers that will substantially improve the behavior of the system by eliminating the possibility of chaos.

We now describe briefly the contents of this paper. In Section 2, we give a one-mode model approximation of the cantilever and from that we extract an approximation for the cantilever–sample model. The dynamical analysis of the forced cantilever–sample system is carried out in Section 3. This section will include the analysis of the effect of feedback on the qualitative behavior of the system, and how a controller can be implemented to eliminate the possibility of chaos in the system. Finally, we draw our conclusions in Section 4.

☆This paper was not presented at any IFAC meeting. This paper was recommended for publication in revised form by Associate Editor Li-Chen Fu under the direction of Editor K. Furuta.

* Corresponding author. Tel.: 001-805-893-2704; fax: 001-805-893-8651.

E-mail address: dahleh@shams.ucsb.edu (M. Dahleh)

PII: S0005-1098(99)00077-1

2. Model description

As has been stated before, the cantilever is at the heart of the detection scheme employed by the atomic force microscope. It is essential that the dynamics of the cantilever be fully understood, before attempting to unfold the complex dynamics which is introduced due to the cantilever–sample interaction. We utilize a one-mode approximation of the multi-mode model developed to study the cantilever–sample interaction.

2.1. Cantilever–sample interaction

The cantilever–sample interaction can be modeled as shown in Fig. 1. The cantilever is modeled as a single spring–mass system with the stiffness of the spring being k and the equivalent mass m. The cantilever interacts with the sample via a tip that is mounted on the cantilever. The cantilever–tip–sample system is modeled by a sphere of radius R and mass m, which is suspended by a spring of stiffness k. We will frequently refer to the mass m as being the tip of the cantilever.

The tip–sample interaction is modeled by an interaction potential which is given by (Israelachvili, 1985)

$$-\frac{AR}{6(Z+x)}, \tag{1}$$

where Z is the equilibrium position of the tip measured from a reference where the sample is positioned in the absence of the sample, x is the displacement of the tip measured from this equilibrium position with the upward direction as the positive direction. This potential models the attraction of a tip of radius R made of material with density ρ_1 by a sample of density ρ_2. The interaction potential is obtained under the assumption that the radius of the tip is much larger than the separation of the tip from the sample. In addition, it models the attractive interaction only and neglects the repulsive part of the potential. $A=\pi^2 Q\rho_1\rho_2$ is the Hamaker constant, where Q is the interaction constant (aqueous solute concentration in mole fraction units (mol/dm^3/55.5)) (Israelachvili, 1985). Typical values that are found in AFM applications are $R=1500$ Å, $A=10^{-19}$ J, and $k=0.0167$ N/m. Thus, the potential for the tip-sample assembly is given by

$$V(x,Z)=-\frac{AR}{6(Z+x)}+\frac{1}{2}kx^2. \tag{2}$$

The net energy of the system scaled by the effective mass m of the cantilever is given by $H(x,\dot{x},Z)$ with

$$H(x,\dot{x},Z)=\frac{1}{2}\dot{x}^2+\frac{1}{2}\omega_1^2x^2-\frac{D\omega_1^2}{(Z+x)}, \tag{3}$$

where, $\omega_1=\sqrt{k/m}$ is the first modal frequency of the system and $D=AR/6k$. Note that H is the Hamiltonian of the system, and therefore is a constant of the dynamics (invariant of motion) since there is no dissipation.

Let $x_1=x$ and $x_2=\dot{x}$. The dynamics of the tip–sample system derived from the above Hamiltonian is given below ($\dot{x}_1=\partial H/\partial x_2$ and $\dot{x}_2=-(\partial H/\partial x_1)$)

$$\dot{x}_1=x_2, \tag{4}$$

$$\dot{x}_2=-\omega_1^2x_1-\frac{D\omega_1^2}{(Z+x_1)^2}. \tag{5}$$

The actual system is both damped and forced, and therefore it is not Hamiltonian. We assume that the damping and external forcing are small enough so that we can think of the actual system as a perturbed Hamiltonian system. Hence, the study of the Hamiltonian (unperturbed) system is very important, as the trajectories of this system will be used (as we will see later) to study the behavior of the perturbed system.

If $x>0$ then the spring force and the vdW force both are directed towards the sample and therefore there will be no fixed points in this region. If $x<0$ the spring force and the vdW force are directed in opposite directions and therefore there is a possibility of fixed points.

The tip will not move if it is at a point where its velocity is zero and the spring force is equal to the vdW force in magnitude. If such a point exists, then it is called a fixed or equilibrium point. However, if Z is small enough, the system will not have fixed points because the vdW force will be larger than the spring force for $x<0$. In this case, the surface snaps the tip into contact.

Next, we find the critical value of Z below which snapping occurs. We will also show that if Z is larger than this critical value then we have two fixed points above the surface.

At the fixed point the acceleration and the velocity of the tip must be equal to zero. Hence, to find the fixed

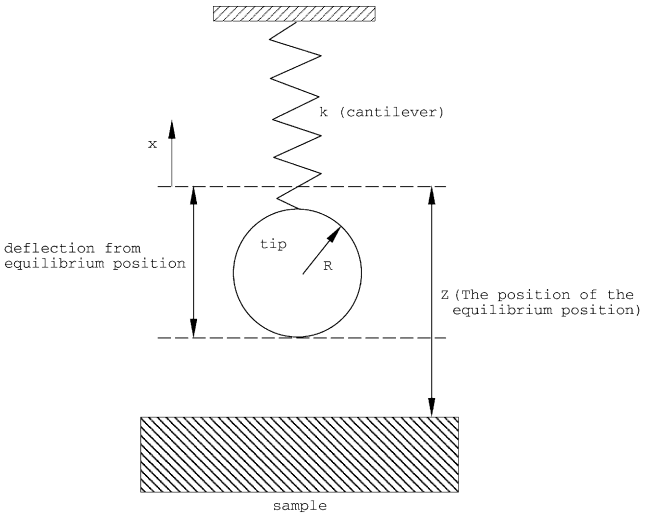

Fig. 1. Tip-sample model.

points of the system we set $\dot{x}_1$ and $\dot{x}_2$ to zero in Eqs. (4) and (5). $\dot{x}_1 = 0$ implies that $x_2 = 0$, and $\dot{x}_2 = 0$ gives

$$x_1^3 + Bx_1^2 + Cx_1 + D = 0, \tag{6}$$

where, $B = 2Z$ and $C = Z^2$. We will find the roots of this polynomial as a function of Z and D. Define

$$p = C - \frac{B^2}{3} = -\frac{Z^2}{3}, \tag{7}$$

$$q = D - \frac{BC}{3} + \frac{2B^3}{27} = D - \frac{2Z^3}{27}, \tag{8}$$

$$R_r = \frac{p^3}{27} + \frac{q^2}{4} = \left(\frac{D}{2}\right)^2 - \frac{1}{27}DZ^3. \tag{9}$$

Let $y^3 = -(q/2) \pm \sqrt{R_r}$ and the three cube roots of y^3 be y_i, $i = 1, 2, 3$. Then the three roots of Eq. (6); x_{1i}, $i = 1, 2, 3$ are given by

$$x_{1i} = y_i - \frac{p}{3y_i} - \frac{B}{3}, \quad i = 1, 2, 3. \tag{10}$$

If $R_r < 0$ then y^3 is imaginary, otherwise it is real. Let Z_s be the solution to $R_r = 0$, i.e., the solution to $(D/2)^2 - (1/27)DZ_s^3 = 0$, which implies that $Z_s = \frac{3}{2}(2D)^{1/3}$. We divide the analysis of the dynamics into two cases; $Z \geq Z_s$ and $Z < Z_s$.

3. Dynamical analysis: the case $Z \geq Z_s$

In this section we discuss the important case when $Z \geq Z_s$, and at the end of the section we give a comment concerning the other case. First, we analyze the system when there is no damping and forcing which will form the basis for the study of the perturbed system where the cantilever is forced sinusoidally and damping is present.

If $Z > Z_s$, $R_r < 0$ and y^3 is imaginary, we can write

$$y^3 = -\frac{q}{2} \pm j\sqrt{-R_r} = r^3 e^{\pm j\theta}, \tag{11}$$

where, $r^3 = \sqrt{(q^2/4) - R_r}$ and $\theta = \arctan\sqrt{(-R_r)}/-q/2$. We consider only $+j\theta$ because (as we will see later) $-j\theta$ gives the same results. Thus, the three roots of y^3 are $y_i = re^{j\theta_i}$, where, $\theta_1 = \theta/3$, $\theta_2 = \theta_1 + (2\pi/3)$, and $\theta_3 = \theta_1 + (4\pi/3)$. Therefore, we have

$$\begin{aligned} x_{1i} &= re^{j\theta_i} - \frac{p}{3r}e^{-j\theta_i} - \frac{B}{3} \\ &= r(\cos\theta_i + j\sin\theta_i) - \frac{p}{3r}(\cos\theta_i - j\sin\theta_i) - \frac{B}{3} \\ &= \left(r - \frac{p}{3r}\right)\cos\theta_i - \frac{B}{3} + j\sin\theta_i\left(r + \frac{p}{3r}\right) \end{aligned} \tag{12}$$

for $i = 1, 2, 3$. Note that $r^3 = \sqrt{(q^2/4) - R_r} = Z^3/27$. Therefore, $r = Z/3$ and we get

$$r + \frac{p}{3r} = \frac{Z}{3} - \frac{-Z^2/3}{Z} = 0 \quad (Z > 0). \tag{13}$$

Thus, the roots of (6) are real for $Z > Z_s$ and they are given by

$$x_{1i} = -\frac{2Z}{3}(1 - \cos\theta_i). \tag{14}$$

Note that θ_i appears in the expression above only as $\cos\theta_i$ which is an even function of θ_i. Therefore, in Eq. (11) we can restrict the analysis to the roots of $y^3 = r^3 e^{j\theta}$. Thus, the fixed points for the system when $Z > Z_s$ are given by $(x_{1i}, 0)$, where, x_{1i}, $i = 1, 2, 3$ are given by Eq. (14).

At the fixed point, the vdW force $(mD\omega_1^2)/(Z + x_1)^2$ and the spring force kx_1 must be equal in magnitude and opposite in direction. In other words, for a fixed point to exist at $(x_1, 0)$ the following relation must hold:

$$-kx_1 = \frac{mD\omega_1^2}{(Z + x_1)^2}. \tag{15}$$

Note that when $Z = Z_s$, $R_r = 0$ and $\theta = \pi$. Thus, $\theta_1 = \pi/3, \theta_2 = \pi$, and $\theta_3 = 5\pi/3$. Therefore, $x_{11} = -(Z_s/3)$, $x_{12} = -(4Z_s/3)$, and $x_{13} = -(Z_s/3)$. x_{11} and x_{13} are equal and are located above the surface. x_{12} lies below the surface and thus has no practical significance. The spring force is equal to the vdW force at only one point above the surface, namely $-Z_s/3$. This means that the spring force is the tangent of the vdW force at the point $-Z_s/3$.

If $Z > Z_s$ then it is clear that $\theta \in (0, \pi)$, and thus $\theta_1 \in (0, \pi/3)$, $\theta_2 \in (2\pi/3, \pi)$, and $\theta_3 \in (4\pi/3, 5\pi/3)$. This

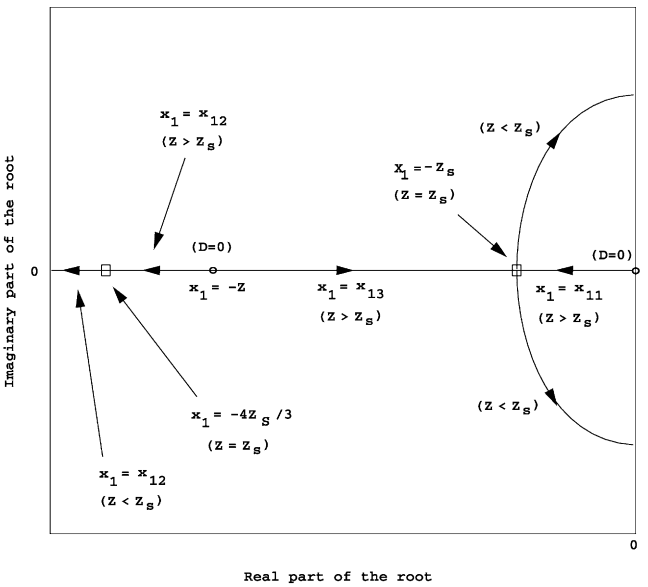

Fig. 2. Root locus plot of the roots of Eq. (6).

implies that $x_{11} \in (-Z_s/3, 0)$, $x_{12} \in (-4Z_s/3, -Z)$, and $x_{13} \in (-Z, -Z_s/3)$. Thus, we have two fixed points above the surface. Note that as Z increases the points x_{11} and x_{13} move towards zero and the surface, respectively.

As Z goes to ∞, θ goes to zero since $\sqrt{(-R_r)}/-q/2$ goes to zero with positive $-q/2$. Hence, x_{11} goes to zero, x_{12} goes to the surface from below, and x_{13} goes to the surface from above. There is a fixed point at zero because the vdW force is equal to zero there. Since Z goes to ∞, the spring force is larger than the vdW force at any point between the surface and $x_{11} = 0$. When the tip gets closer to the surface the vdW force increases rapidly and it becomes equal to the spring force at a point that approaches the surface. A summary of the above analysis can be seen in Fig. 2.

3.1. Phase portrait

We will examine the nature of the fixed points by linearizing the system as given below

$$\begin{pmatrix} \dot{x}_1 \\ \dot{x}_2 \end{pmatrix} = \begin{pmatrix} 0 & 1 \\ -\omega_1^2 + \dfrac{2D\omega_1^2}{(Z + x_{1i})^3} & 0 \end{pmatrix} \begin{pmatrix} x_1 \\ x_2 \end{pmatrix}, \quad i = 1, 3. \tag{16}$$

For $Z > Z_s$ the eigenvalues of the linearized system are purely imaginary at $x_1 = x_{11}$, and real with equal magnitude and opposite sign at $x_1 = x_{13}$. Thus, the fixed point x_{11} is a center, whereas x_{13} is a saddle point. From now on, we will denote x_{11} and x_{13} by x_c and x_s, respectively.

Fig. 3 shows the phase portrait of the system. There is a homoclinic orbit connected to itself at the point $(x_s, 0)$. This homoclinic orbit is filled with periodic orbits around the center $(x_c, 0)$. When $x_1 < x_s$ the tip accelerates towards the surface and hits it with a large velocity (snapping). Denote the maximum position on the x_1 axis that the homoclinic orbit obtains by x_e. If $x_s < x_1 < x_e$ and x_2 is not too large, the tip oscillates around the center. If x_2 is large enough, then the tip will have extra energy, so it will pass x_s accelerating towards the surface.

3.2. Homoclinic solution

In this section, we find an analytic relation between time and x_1 for the homoclinic orbit. Since the Hamiltonian of the system is an invariant of motion, it is constant along the trajectories of the system. Thus, the homoclinic solution satisfies the following equation:

$$H(x_1, x_2, Z) = H(x_s, 0, Z). \tag{17}$$

If we let $c = H(x_s, 0, Z)$, we have

$$\frac{1}{2}x_2^2 + \frac{1}{2}\omega_1^2 x_1^2 - \frac{D\omega_1^2}{(Z + x_1)} = c. \tag{18}$$

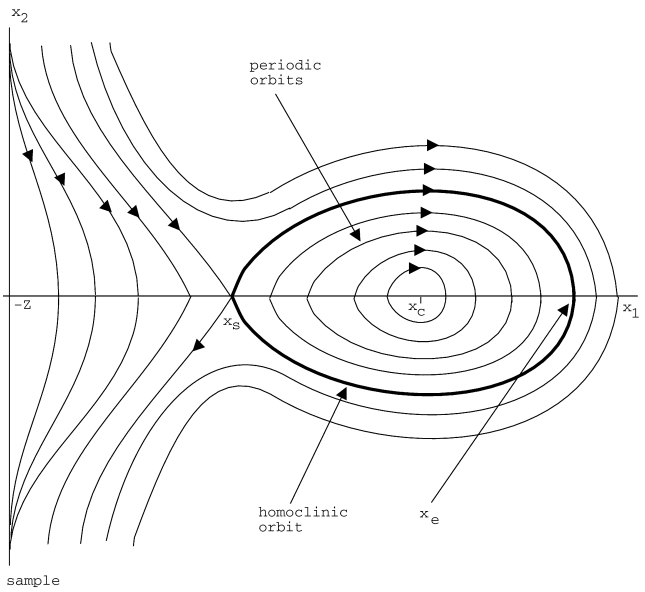

Fig. 3. Phase portrait.

This can be written as

$$x_2^2 = -\omega_1^2 \frac{x_1^3 + Zx_1^2 - (2c/\omega_1^2)x_1 - 2(D + (c/\omega_1^2)Z)}{Z + x_1}. \tag{19}$$

The roots of the numerator of the right-hand side of this expression are x_s (two repeated roots) and x_e. This is because the homoclinic orbit crosses the x_1 axis at the points x_s and x_e. Since for $H(x_1, x_2, Z) = c$, the solution exits on both sides of the saddle point (since x_s has stable and unstable manifolds), x_s has to be a repeated root so that x_2^2 is positive around x_s. Therefore, we have

$$\begin{aligned} x_1^3 + Zx_1^2 - \frac{2c}{\omega_1^2}x_1 - 2\left(D + \frac{c}{\omega_1^2}Z\right) &= (x_1 - x_s)^2(x_1 - x_e) \\ &= x_1^3 - (x_e + 2x_s)x_1^2 + (2x_s x_e + x_s^2)x_1 - x_s^2 x_e. \end{aligned} \tag{20}$$

Equating the coefficients of x_1^2 in Eq. (20) we have, $Z = -(x_e + 2x_s)$. Solving for x_e, we get $x_e = -Z - 2x_s = -x_s - (Z + x_s)$. Using Eq. (6) it is easy to show that the other coefficients in Eq. (20) are equal which justifies our claim.

Note that x_e is equal to the difference between the two dimensions that are shown in Fig. 4. From Eq. (19) we have

$$x_2 = \pm \omega_1 (x_1 - x_s)\sqrt{\frac{x_e - x_1}{Z + x_1}}, \quad (x_s \le x_1 \le x_e). \tag{21}$$

To obtain the homoclinic orbit we will solve the equations of motion and assume that the time origin t_0

is chosen so that $x_1(t_0) = x_e$. It is clear that if $t \geq t_0$ then the trajectory is such that $x_2(t) \leq 0$. Therefore, we have for $t \geq t_0$

$$\dot{x}_1 = x_2 = -\omega_1(x_1 - x_s)\sqrt{\frac{x_e - x_1}{Z + x_1}}, \quad (x_s \leq x_1 \leq x_e). \tag{22}$$

(Note that the right-hand side is always negative in the region of interest.) Similarly, if $t < t_0$ then $x_2 > 0$ and we have

$$\dot{x}_1 = x_2 = +\omega_1(x_1 - x_s)\sqrt{\frac{x_e - x_1}{Z + x_1}}, \quad (x_s \leq x_1 \leq x_e). \tag{23}$$

We will now solve for $x_1(t)$ when $t \geq t_0$. Separation of variables in Eq. (22) yields

$$\frac{1}{x_1 - x_s}\sqrt{\frac{Z + x_1}{x_e - x_1}}\,dx_1 = -\omega_1\,dt. \tag{24}$$

Substituting $u = x_1 - x_s$ in Eq. (24), we have

$$\frac{1}{\sqrt{P}}du + \frac{Z + x_s}{u\sqrt{P}}du = -\omega_1\,dt, \tag{25}$$

where, $P = [(Z + x_s) + u][(x_e - x_s) - u]$. Note that when $t = t_0$, $u = x_e - x_s$. Integrating (25) from time t_0 to time t and substituting back $x_1 = u + x_s$, we have (see Gradshteyn & Ryzhik, 1980)

$$-\arcsin\frac{x_1 + Z + x_s}{x_s} - \sqrt{\frac{Z + x_s}{-Z - 3x_s}} * \ln - \left(\frac{(Z + x_s)(-Z - 3x_s) + (-Z - 2x_s)(x_1 - x_s) + \sqrt{(Z + x_s)(x_e - x_s)P}}{x_s(x_1 - x_s)}\right) - \frac{\pi}{2} = -\omega_1(t - t_0). \tag{26}$$

Therefore, if the initial condition at time t_0 for the system is $(x_e,0)$ then for $t \geq t_0$, $x_1(t)$ is obtained from Eq. (26) and

$$x_2 = -\omega_1(x_1 - x_s)\sqrt{\frac{x_e - x_1}{Z + x_1}}. \tag{27}$$

Similarly, if the initial condition at time t_0 for the system is $(x_e,0)$ then for $t < t_0$, $x_1(t)$ is obtained from the following equation:

$$-\arcsin\frac{x_1 + Z + x_s}{x_s} - \sqrt{\frac{Z + x_s}{-Z - 3x_s}} * \ln - \left(\frac{(Z + x_s)(-Z - 3x_s) + (-Z - 2x_s)(x_1 - x_s) + \sqrt{(Z + x_s)(x_e - x_s)P}}{x_s(x_1 - x_s)}\right) - \frac{\pi}{2} = +\omega_1(t - t_0), \tag{28}$$

and $x_2(t)$ is obtained from

$$x_2 = +\omega_1(x_1 - x_s)\sqrt{\frac{x_e - x_1}{Z + x_1}}. \tag{29}$$

Note that for a given x_1 in the desired range of interest $x_2(-\tau) = -x_2(\tau)$ for $\tau = t - t_0$. Therefore, x_2 is an odd function of τ. Thus, we have obtained a complete description of the homoclinic orbit.

3.3. The perturbed system

In most AFMs the cantilever motion is damped due to the surrounding air. In addition, the cantilever is forced by a small sinusoidal signal $mf\cos\omega t$, where, ω takes values around the natural frequency ω_1 of the system. The differential equation for the perturbed system can be written as

$$\dot{x}_1 = x_2, \tag{30}$$

$$\dot{x}_2 = -\omega_1^2 x_1 - \frac{D\omega_1^2}{(Z + x)^2} + f\cos\omega t - \mu x_2, \tag{31}$$

where we have assumed that the damping force per unit mass is μx_2. Given a small enough ε, define γ and δ such that $\varepsilon\gamma = f$ and $\varepsilon\delta = \mu$. Using suspension (i.e., consider the time to be a new state variable, ϕ), we have

$$\dot{x}_1 = x_2, \tag{32}$$

$$\dot{x}_2 = -\omega_1^2 x_1 - \frac{D\omega_1^2}{(Z + x)^2} + \varepsilon(\gamma\cos\phi - \delta x_2), \tag{33}$$

$$\dot{\phi} = \omega, \tag{34}$$

where $\phi(t) = \omega t + \phi_0$. Define

$$g(x_1,x_2,\phi) = \begin{pmatrix} 0 \\ \gamma\cos\phi - \delta x_2 \end{pmatrix}. \tag{35}$$

Thus, the Hamiltonian system described previously is now perturbed by εg. The next step is to study the dynamics of the perturbed system. To achieve this goal, we will study the Melnikov function for the perturbed system.

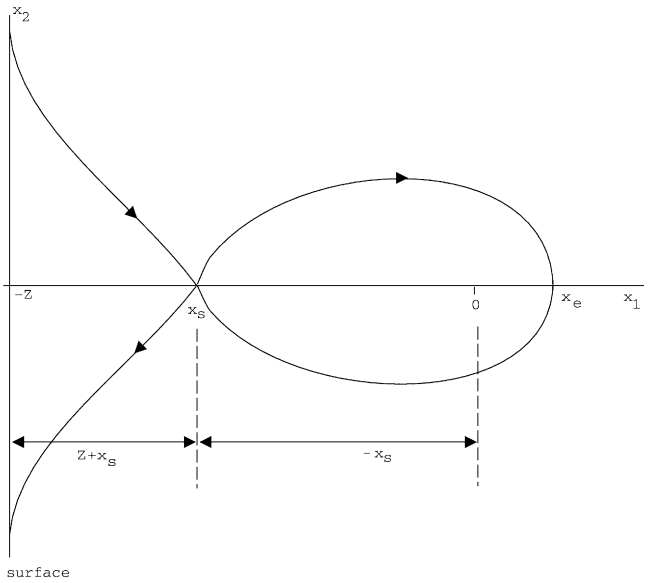

Fig. 4. Homoclinic orbit.

3.4. Melnikov function

Since the system that we are considering is a time-periodic perturbation of a Hamiltonian system, Melnikov's method can be used to describe how the homoclinic orbit breaks up in the presence of the perturbation. The Melnikov function is defined as (Wiggins, 1990)

$$M(t_0,\phi_0) = \int_{-\infty}^{\infty} DH(x_{1h}(\tau), x_{2h}(\tau)) g(x_{1h}(\tau), x_{2h}(\tau), \phi(\tau + t_0))\,\mathrm{d}\tau, \tag{36}$$

where, $DH(x_1, x_2) = ((\partial H/\partial x_1)(\partial H/\partial x_2))$, and $x_{1h}(\tau)$ and $x_{2h}(\tau)$ are the homoclinic solution as given by Eqs. (26)–(29). Therefore,

$$\begin{aligned} M(t_0,\phi_0) &= \int_{-\infty}^{\infty} x_{2h}(\tau)(\gamma\cos(\omega\tau + \omega t_0 + \phi_0) - \delta x_{2h}(\tau))\,\mathrm{d}\tau \\ &= -2\delta\int_0^{\infty} x_{2h}^2(\tau)\,\mathrm{d}\tau - 2\gamma\sin(\omega t_0 + \phi_0) \\ &\quad \int_0^{\infty} x_{2h}(\tau)\sin\omega\tau\,\mathrm{d}\tau. \end{aligned} \tag{37}$$

The last equality holds because $x_{2h}(\tau)$ is an odd function of τ, assuming $x_{1h} = x_e$ at $t = t_0$. Let $a_d = -2\int_0^{\infty} x_{2h}^2(\tau)\,\mathrm{d}\tau$ and $a_s = -2\int_0^{\infty} x_{2h}(\tau)\sin\omega\tau\,\mathrm{d}\tau$. Hence,

$$M(t_0,\phi_0) = a_d\delta + a_s\gamma\sin(\omega t_0 + \phi_0). \tag{38}$$

The Melnikov function is a signed measure of the distance between the stable and unstable manifolds for the perturbed system. The manifolds intersect if the Melnikov function has simple zeros and is independent of ε. The intersection of manifolds indicates the presence of chaos (Wiggins, 1990). The Melnikov function will have zeros if and only if $(\delta/\gamma) \le |a_s/a_d|$. Define $(\delta/\gamma)_{cr} = |a_s/a_d|$. If $(\delta/\gamma) > (\delta/\gamma)_{cr}$ then $M(t_0,\phi_0)$ has no zeros, otherwise it does. ϕ_0 fixes a Poincaré section, while t_0 specifies a point on the unperturbed homoclinic orbit. Every zero of the Melnikov function corresponds to an intersection (within order ε) of the stable and unstable manifolds (Wiggins, 1990, 1992). Note that if $(\delta/\gamma) \le (\delta/\gamma)_{cr}$ then the two manifolds intersect at an infinite number of points for every Poincaré section ϕ_0.

3.5. Qualitative behavior

In this subsection, we define variables which facilitate the study of the qualitative behavior of the system. Let $T = \omega_1 t$ (time scale) and divide the left and right-hand sides of Eqs. (30) and (31) by Z_s to get

$$\xi_1' = \xi_2, \tag{39}$$

$$\xi_2' = -\xi_1 - \frac{d}{(\alpha + \xi_1)^2} + \varepsilon(\Gamma\cos\Omega T - \Delta\xi_2), \tag{40}$$

where, $\xi_1 = x_1/Z_s$, $\xi_2 = x_2/\omega_1 Z_s$, $d = 4/27$, $\Gamma = \gamma/\omega_1^2 Z_s$, $\Delta = \delta/\omega_1$, $\alpha = Z/Z_s$, and $\Omega = \omega/\omega_1$. The prime denotes the derivative with respect to T. In the new coordinates there is no explicit dependence on D and ω_1 (note that the same γ and δ give different Γ and Δ for different values of D and ω_1). In other words, there is no explicit dependence on the material properties and the dimensions of the cantilever and tip. The quantitative results differ by scaling factors depending on these two parameters.

The new system looks like the old system with Z replaced by α, D by d and ω_1 by 1. Hence, all of the previous analysis applies to the new system with the new factors. The Melnikov function in the new coordinates is

$$M(T_0,\phi_0) = A_d\Delta + A_s\Gamma\sin(\Omega T_0 + \phi_0), \tag{41}$$

where,

$$A_d = -2\int_0^{\infty} \xi_{2h}^2(\tau)\,\mathrm{d}\tau,$$

and

$$A_s = -2\int_0^{\infty} \xi_{2h}(\tau)\sin\Omega\tau\,\mathrm{d}\tau.$$

Define the critical value of Δ/Γ as $(\Delta/\Gamma)_{cr} = |A_s/A_d|$. It is easy to verify that

$$\left(\frac{\delta}{\gamma}\right)_{cr} = \frac{1}{\omega_1 Z_s}\left(\frac{\Delta}{\Gamma}\right)_{cr}. \tag{42}$$

$(\Delta/\Gamma)_{cr}$ is computed numerically for different values of $\alpha > 1$ and Ω around 1. The results are plotted as shown in Fig. 5. If the material properties and dimensions of the cantilever and tip are given, then we first compute Z_s and

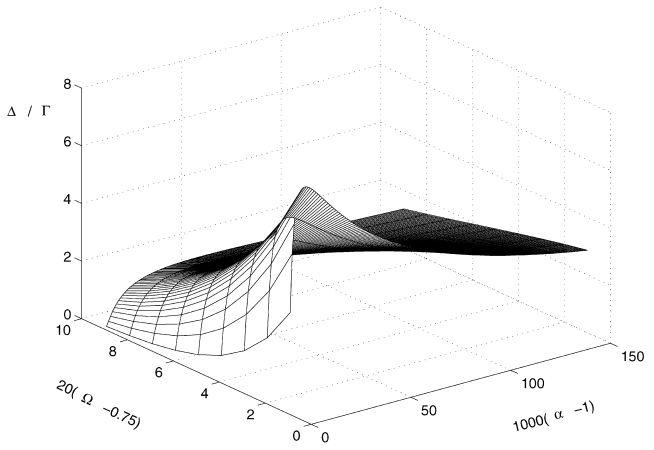

Fig. 5. $(\Delta/\Gamma)_{cr}$ surface. The region below the surface is the region where chaos exists in the system. The region above the surface is the region of no chaos.

ω_1 and then with the appropriate scaling transform Fig. 5 to a figure with δ/γ, Z, and ω as coordinates.

Intersection of the stable and the unstable manifolds occurs for points which lie below the surface plotted in Fig. 5. As α increases the system tends to the spring–mass–damper system behavior which does not exhibit chaotic motion when it is perturbed by a sinusoidal external forcing, and the exact trajectories of the system can be found analytically. When Z is small enough, i.e., α is close enough to 1, again there will be no chaotic motion because x_s and x_e get close enough to each other such that small perturbations cause the motion to be outside the homoclinic orbit and the surface will snap the tip into contact. If we fix α then as Ω increases the chance for chaos decreases.

3.6. State feedback control

In most AFMs the state x_1 (position) is measured, and the state x_2 (velocity) can be estimated. This makes it possible to apply a force of the form $u = k_p x_1 + k_v x_2$ to the cantilever. In this case, the state equations of the system are written as

$$\dot{x}_1 = x_2, \tag{43}$$

$$\begin{aligned}\dot{x}_2 = &-\omega_1^2 x_1 - \frac{D\omega_1^2}{(Z+x_1)^2} + \varepsilon(\gamma\cos\omega t - \delta x_2)\\ &+\frac{k_p}{m}x_1 + \frac{k_v}{m}x_2\\ = &-\omega_{n1}^2 x_1 - \frac{D_1\omega_{n1}^2}{(Z+x_1)^2} + \varepsilon(\gamma\cos\omega t - \delta_1 x_2),\end{aligned} \tag{44}$$

where $(\omega_{n1})^2 = (k_1/m)$ with $k_1 = k - k_p$, $D_1 = (AR/6k_1)$, and $\delta_1 = \delta - (1/\varepsilon)(k_v/m)$. We can see that applying the above state feedback control is equivalent to changing k and δ in the system independently. Note that $k_1 = 0$ means that the tip accelerates towards the sample regardless of the initial condition. If $k_1 < 0$ there is only one equilibrium point above the sample ($x_1 > 0$,0) which is unstable. We will restrict our analysis to the case when $k_1 > 0$ and $\delta_1 \geq 0$.

Now, by fixing $k = k_0$ and $\delta = \delta_0$ we get the point $(\alpha_0, \Omega_0, (\Delta/\Gamma)_0)$ in a three-dimensional space, where $\alpha_0 = Z/Z_{s0}$ with $Z_{s0} = 3/2(2(AR/6k_0))^{1/3}$, $\Omega_0 = \omega/\omega_{10}$ with $\omega_{10} = \sqrt{k_0/m}$, and $(\Delta/\Gamma)_0 = \omega_{10}Z_{s0}(\delta_0/\gamma)$. Let $k = \rho k_0$, where $\rho > 0$. It is easy to see that this corresponds to the point $(\rho^{1/3}\alpha_0, \rho^{-1/2}\Omega_0, \rho^{1/6}(\Delta/\Gamma)_0)$. Varying ρ is equivalent to varying k. The variation of ρ induces a variation of the point $(\rho^{1/3}\alpha_0, \rho^{-1/2}\Omega_0, \rho^{1/6}(\Delta/\Gamma)_0)$ on a one-dimensional curve in a three-dimensional space. Each curve is characterized by a fixed ω, γ, Z, and δ, and each point on the curve corresponds to a particular k. As k increases the point moves in the $+\alpha$, $-\Omega$, $+\Delta/\Gamma$ direction, and vice versa. Fig. 6 shows curves of constant ω, γ, Z, and δ along with the $(\Delta/\Gamma)_{cr}$ surface. Recall that when the operating point is on or under this surface the stable and unstable manifolds intersect, otherwise they do not. If the curve of constant ω, γ, Z, and δ intersects the $(\Delta/\Gamma)_{cr}$ surface, then we can move the operating point from one side of this surface to the other by changing k appropriately. Note that by varying k the $(\delta/\gamma)_{cr}$ surface shifts in the Z and ω coordinates, while the $(\Delta/\Gamma)_{cr}$ surface is fixed in the α and Ω coordinates. Clearly, with the aid of this diagram we can select the controller parameter k_p to suppress the possibility of chaos.

Now, we will analyze the effect of the controller term k_v. Let $k = k_0$ be a fixed constant and let $\delta = \rho\delta_0$. These nominal conditions give the point $(\alpha_0, \Omega_0, \rho(\Delta/\Gamma)_0)$. By varying ρ (δ) the operating point moves in the vertical (Δ/Γ) direction. As δ increases the operating point moves in the $+\Delta/\Gamma$, and vice versa. Thus, we can move the operating point from one side of the $(\Delta/\Gamma)_{cr}$ surface to the other by changing δ appropriately. This procedure gives us the controller term k_v which results in the elimination of the possibility of chaos.

In summary, the tools of Melnikov theory are used to provide a procedure for the design of a controller of the

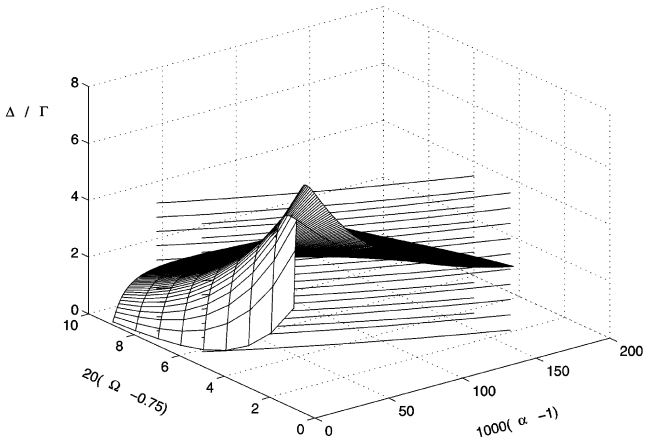

Fig. 6. Curves of constant ω, γ, Z, and δ and the $(\Delta/\Gamma)_{cr}$ surface.

form $u = k_v x_1 + k_p x_2$ that will eliminate chaos if it exists when $u = 0$.

Finally, for the case when $Z = Z_1 < Z_s$, the vdW force is greater than the spring force whenever $x_1 < 0$. Hence, there are no fixed points above the surface and the corresponding two roots are imaginary as shown in Fig. 2. In this case, the surface snaps the tip into contact.

4. Conclusions

A mathematical model for the cantilever–sample interaction in the AFM was utilized to explore the dynamical behavior of the cantilever. It is shown that it is possible for chaos to exist in the system depending on the extent of damping and forcing. The region in which chaos exists was found. It was shown that feedback control can be used to eliminate the possibility of chaos. Ongoing research involves the experimental validation of the predictions, and the implementation of control to eliminate chaos.

Acknowledgements

This research was partly supported by NSF ECS-9632820, NSF ECS-9733802 and AFOSR F49620-97-1-0168.

References

Burnham, N. A., Kulik, A. J., Gremaud, G., & Briggs, G. A. D. (1995). Nanosubharmonics: The dynamics of small nonlinear contacts. *Physical Review Letters*, *74*, 5092–5059.

Gradshteyn, I. S., & Ryzhik, I. M. (1980). *Table of integrals, series, and products*. New York: Academic Press.

Israelachvili, J. N. (1985). *Intermolecular and surface forces*. New York: Academic Press.

Sarid, D. (1994). *Scanning force microscopy*. New York: Oxford University Press.

Wiggins, S. (1992). *Chaotic transport in dynamical systems*. Berlin: Springer.

Wiggins, S. (1990). *Introduction to applied nonlinear dynamical systems and chaos*. Berlin: Springer.

M. Sami Ashhab received the B.S. degree in mechanical engineering from The University of Jordan, Amman, in 1994 and the M.S. and Ph.D. degrees in mechanical engineering from The University of California, Santa Barbara, in 1996 and 1998, respectively.

He is currently employed by Meta-Heuristics, LLC. to participate in developing a software to analyze databases for the purpose of modeling and optimization.

Murti V. Salapaka was born on January 30, 1969. He received the B.Tech degree from Indian Institute of Technology, Madras, in 1991, and the M.S. and Ph.D. degrees from University of California, Santa Barbara in 1993 and 1997, respectively. Since 1997, he has been with the Electrical Engineering Department at Iowa State University as an Assistant Professor. His research interests are in robust control, dynamical systems and scanning probe microscopy. He is a recipient of the 1997 CAREER award from National Science Foundatation. He is a member of IEEE.

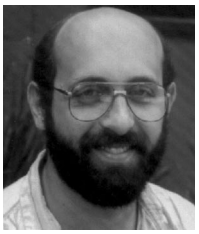

Mohammed Dahleh was born on February 12, 1961. He received the B.S.EE. degree from Texas A&M University, in 1983, and the M.A. and Ph.D. degrees from Princeton University, in 1986 and 1987, respectively. From 1987 to 1990, he was an Assistant Professor at the Department of Electrical Engineering at Texas A&M University. Since January 1991, he has been with the Mechanical and Environmental Engineering Department at the University of California, Santa Barbara as an Assistant Professor (1991–1993), Associate Professor (1993–1995), and since July, 1995 as a Professor. He is currently the Vice Chairman of the Department of Mechanical Engineering and the Research Director of the Center for Control Engineering and Computation. His research interests are in robust control, and applications of control to micro-scale mechanical problems. His research is funded by the National Science Foundation, Air Force Office of Scientific Research, Ford Motor Company, and NATO. He served as an associate editor for the journals: Systems and Control Letters, IEEE Transactions on Automatic Control, and the ASME Journal on Dynamic Systems Measurement and Control. He is a member of ASME, IEEE, and SIAM.

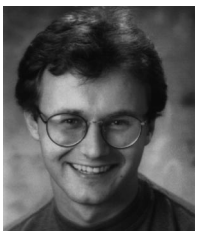

Igor Mezić was born on June 18, 1967. He received the Dipl. Ing. in Mechanical Engineering degree from University of Rijeka, Croatia in 1990, and the Ph.D. degree from the California Institute of Technology, in 1994. From 1994 to 1995, he was a Postdoctoral Fellow at the Mathematics Institute of the University of Warwick, UK. Since July 1995, he has been with the Mechanical and Environmental Engineering Department at the University of California, Santa Barbara as an Assistant Professor. He is a member of the Center for Control Engineering and Computation. His research interests are in dynamical systems, and applications of dynamical systems theory to mixing, micro-scale mechanical problems and axial compression systems. His research is funded by the National Science Foundation, Air Force Office of Scientific Research, Office of Naval Research, Propulsion Research Institute, and NATO. He is a member of SIAM and APS.